

Nonaxial octupole deformations in light $N = Z$ nuclei at high spins

Takeshi Tanaka and Rashid G. Nazmitdinov

Bogoliubov Laboratory of Theoretical Physics, Joint Institute for Nuclear Research
141980 Dubna Moscow Region, Russia.

Kazuo Iwasawa

Information Processing Center, Hiroshima University
Hiroshima 739-8526, Japan.

9 Apr. 2000

Abstract

High spin states of ^{32}S and ^{56}Ni are investigated by means of the cranking Hartree-Fock method with the Gogny interaction without imposing a restriction on the axial reflection symmetry. It was found that a non-axial octupole deformation of the Y_{31} type becomes important in the yrast states of ^{32}S . A similar effect is predicted for the nucleus ^{56}Ni .

PACS number(s): 21.60-n; 21.60.Jz; 27.30.+t; 27.40.+z

1 Introduction

One of the most important concepts in the many-body theory of finite Fermi systems is the mean field approach. In fact, many phenomena observed in nuclei can be explained by means of a spontaneous symmetry breaking mechanism which leads to a mean field solution that does not obey symmetries of the original many-body Hamiltonian [1, 2]. A nucleus with a partially filled highest shell spontaneously deforms in such a way that a lower energy minimum is achieved, and thus a non-spherical equilibrium shape is attained. Coriolis forces may cause a similar effect for a nucleus which has a spherical shape in a ground state. In particular, a strong coupling of normal and intruder states near the Fermi surface at large rotational frequencies can lead to a superdeformed or to an octupole deformed shape for certain combinations of protons and neutrons [3]. The most practical method for the analysis of nuclear shapes is a phenomenological macroscopic-microscopic method (MMM) which combines the liquid drop model describing the bulk properties of nuclear matter and the Strutinsky Shell Correction method providing the description of quantum shell effects of phenomenological potentials [2]. The more fundamental approach is based on self-consistent Hartree-Fock (HF) calculations once a particular choice of nucleon-nucleon interaction has been made. A commonly used inter-nucleon force is that of Skyrme. While the HF+Skyrme approach describes major features of nuclei quite well, it does not completely take into account the pairing correlations. In addition, various sets of parameters for Skyrme forces may not provide a definite answer in some cases. The Hartree-Fock-Bogoliubov (HFB) method with the Gogny forces resolves these problems quite effectively. Furthermore, it has the same prediction power as the MMM [4].

In recent years a lot of experimental and theoretical efforts has been devoted to the analysis of superdeformed (SD) bands in different mass region [3, 5, 6, 7, 8]. On the other hand, the study of octupole degrees of freedom is also a topical subject in the nuclear structure physics [9, 10]. It turns out that octupole deformations are significant for superdeformed nuclei as well as for normal-deformed (ND) nuclei. Most of these studies were restricted to the axial octupole deformation proportional to the Y_{30} term in the octupole family. The reason for this is primarily computational complications arising as a result of the extra degree of freedom introduced by non-axial octupole deformations. However, during the last few years some remarkable results have been reported. It was found that Y_{31} and Y_{32} components resulted in the lowest energy octupole vibrations for oblate and prolate superdeformed shapes and therefore may have consequences for octupole instability [11, 12, 9]. Calculations using the MMM with the Woods–Saxon potential predicted the importance of the banana-type Y_{31} deformation for highly deformed nuclei [13], while the Y_{32} deformation has been found to be important in the ^{222}Ra nucleus [14]. The self-consistent HF+Skyrme calculations [15] suggest the softness of the oblate states in $A \sim 80$ nuclei against the Y_{33} deformation in the ground states. The self-consistent cranking HF+Skyrme approach [16] predicts that the Y_{31} deformation is important for a correct description of the yrast band of ^{32}S . Moreover, the study of octupole deformations sheds light on the interplay between a classical chaos and a quantum spectrum of finite Fermi systems [17, 18, 19]. Guided by thorough investigation of non-axial octupole deformations in a harmonic oscillator model [20], we aim to analyze how symmetries break at high spins in the cranking HFB approach with the Gogny interaction. In accordance with the octupole instability suggested at particle number $N = 16$ and 28 [20], we choose two $N = Z$ nuclei, ^{32}S and ^{56}Ni . In Sec.2 we review the main features of our model. The discussion of main results is presented in Sec.3 with the conclusion following in Sec.4. In the Appendix we introduce a simple two-level model to understand qualitatively the behavior of the Inglis-Beliaev moment of inertia due to strong octupole coupling between two single-particle (s.p.) states.

2 The Model

As mentioned above, the present self-consistent cranking HFB calculation has been performed with the effective Gogny D1S interaction [21, 22, 23, 24]. This interaction provides a good description of many nuclear properties over the nuclide chart, e.g., ground state energies, odd-even energy differences, electron scattering data [22], fission barriers [24]. Also, a good description is obtained for bulk properties of rotating nuclei in actinide region [25], mercury region [26] and fp-shell region [27]. Our numerical code has been used for the analysis of microscopic dynamics in light rotating nuclei [28, 29, 30]. In these calculations, however, the signature symmetry was conserved (see discussion about different symmetries in rotating nuclei in [10, 31]). The present calculations are performed without assuming *a priori* the axial and signature symmetries. In addition, our Hamiltonian includes the Coulomb interaction and the center of mass correction up to the exchange terms exactly.

The z -axis is taken as a rotational axis in our code. To save the CPU time in numerical calculations, we impose the $\hat{P}e^{-i\pi\hat{J}_z}$ (z -simplex) and the $\hat{P}e^{-i\pi\hat{J}_y}\hat{\tau}$ (\hat{S}_y^T) symmetries [31], where \hat{P} is the parity operator, $e^{-i\pi\hat{J}_i}$ is the rotation operator around the i -axis ($i=y,z$) on angle π , and $\hat{\tau}$ is the time-reversal operator. Due to the z -simplex and \hat{S}_y^T symmetries, the mass asymmetry of nucleus is allowed only along the x -axis. Thus, we solve numerically the following cranking HFB equations:

$$\delta\langle\phi(\omega)|\hat{H} - \lambda_p\hat{Z} - \lambda_n\hat{N} - \omega\hat{J}_z$$

$$+\mu_x \langle \phi(\omega) | \hat{x} | \phi(\omega) \rangle \hat{x} | \phi(\omega) \rangle = 0. \quad (1a)$$

$$\langle \phi(\omega) | \hat{Z} | \phi(\omega) \rangle = Z, \quad \langle \phi(\omega) | \hat{N} | \phi(\omega) \rangle = N, \quad (1b)$$

$$\langle \phi(\omega) | \hat{J}_z | \phi(\omega) \rangle = I, \quad (1c)$$

$$\langle \phi(\omega) | \hat{x} | \phi(\omega) \rangle = 0, \quad (1d)$$

where the Lagrange multipliers λ_p and λ_n are the chemical potentials of proton and neutron fields, respectively (the operators \hat{Z} and \hat{N} are protons and neutrons number operators); the Lagrange multiplier ω is the angular frequency of a collective rotation around the z -axis and \hat{J}_z is the z -component of the angular momentum operator $\hat{\mathbf{J}}$. To keep the center of mass motion fixed, we also impose the quadrupole constraint operator $\mu_x \langle \phi(\omega) | \hat{x} | \phi(\omega) \rangle \hat{x}$ [32] to the Routhian $\hat{R} = \hat{H} - \lambda_p \hat{Z} - \lambda_n \hat{N} - \omega \hat{J}_z$ in the x -axis direction.

The quasi-particle (q.p.) operators

$$\hat{\alpha}_i^\dagger = \sum_k U_{ki} \hat{c}_k^\dagger + V_{ki} \hat{c}_k, \quad (2)$$

where the state $|k\rangle$ is a single-particle basis state (see below), obey the equation of motion

$$[\hat{R}, \hat{\alpha}_i^\dagger] = \epsilon_i(\omega) \hat{\alpha}_i^\dagger \quad (3)$$

which defines the quasi-particle energies $\epsilon_i(\omega)$ and quasi-particle amplitudes U_{ki} and V_{ki} as functions of the rotational frequency ω .

We define the y -axis as the quantization axis of deformation for convenience. Consequently, the quadrupole, β_2 and γ , and octupole, β_{3m} , deformation parameters are defined as

$$\beta_2 \cos \gamma \equiv \frac{4\pi}{5} \frac{\langle r^2 Y_{20}(\theta, \varphi) \rangle}{AR_0^2} \quad (4)$$

$$= \sqrt{\frac{\pi}{5}} \frac{\langle (3y^2 - r^2) \rangle}{AR_0^2},$$

$$\beta_2 \sin \gamma \equiv \frac{4\pi}{5} \frac{\langle r^2 (Y_{22}(\theta, \varphi) + Y_{2-2}(\theta, \varphi)) \rangle}{\sqrt{2} AR_0^2} \quad (5)$$

$$= \sqrt{\frac{3\pi}{5}} \frac{\langle (x^2 - z^2) \rangle}{AR_0^2},$$

$$\beta_{30} \equiv \frac{4\pi}{3} \frac{\langle r^3 Y_{30}(\theta, \varphi) \rangle}{AR_0^3} \quad (6)$$

$$= \sqrt{\frac{7\pi}{9}} \frac{\langle y(5y^2 - 3r^2) \rangle}{AR_0^3},$$

$$\beta_{31} \equiv \frac{4\pi}{3} \frac{\langle r^3 (Y_{31}(\theta, \varphi) - Y_{3-1}(\theta, \varphi)) \rangle}{\sqrt{2} AR_0^3} \quad (7)$$

$$= -\sqrt{\frac{21\pi}{18}} \frac{\langle x(5y^2 - r^2) \rangle}{AR_0^3},$$

$$\beta_{32} \equiv \frac{4\pi \langle r^3(Y_{32}(\theta, \varphi) + Y_{3-2}(\theta, \varphi)) \rangle}{3 \sqrt{2} AR_0^3} \quad (8)$$

$$= \sqrt{\frac{105\pi}{9}} \frac{\langle y(x^2 - z^2) \rangle}{AR_0^3},$$

$$\beta_{33} \equiv \frac{4\pi \langle r^3(Y_{33}(\theta, \varphi) - Y_{3-3}(\theta, \varphi)) \rangle}{3 \sqrt{2} AR_0^3} \quad (9)$$

$$= -\sqrt{\frac{35\pi}{18}} \frac{\langle x(x^2 - 3z^2) \rangle}{AR_0^3},$$

where (r, θ, φ) are spherical coordinates related to the Cartesian coordinates in the rotating frame (x, y, z) as

$$(x, y, z) \equiv (r \sin \theta \cos \varphi, r \cos \theta, r \sin \theta \sin \varphi). \quad (10)$$

All deformations proportional to the odd power of the y coordinate are forbidden in our code due to the \hat{S}_y^T symmetry. Since β_{30} and β_{32} are proportional to the odd y^n terms, we use β_{31} and β_{33} to represent the degree of the non-axial octupole deformation, when the y -axis is the largest axis of a prolate nucleus. Notice that the octupole deformation with a mass asymmetry like a pear shape is also represented by the combination of β_{31} and β_{33} when the x -axis is the largest axis of a prolate nucleus ¹.

The s.p. wave functions have been expanded in a three-dimensional harmonic oscillator basis up to the principal quantum number $N = 8$ for ^{32}S and up to $N = 10$ for ^{56}Ni . The basis has been symmetrized with respect to the z -simplex operation, and eigenfunctions are eigenstates of the \hat{S}_y^T operator (the Goodman basis [33]). Since the ground state shapes of the chosen nuclei are a normal-deformed one for ^{32}S and a spherical one for ^{56}Ni , we use a spherical Cartesian basis with the same range parameters of the Hermite polynomials for all axes. The range parameters have been optimized to reproduce the largest binding energy of each ground state.

To understand the relation between s.p. degrees of freedom and collective effects due to the rotation, we calculate three moments of inertia, the static moment of inertia $\mathcal{J}^{(1)}(\omega) \equiv I/\omega$, the dynamical moment of inertia $\mathcal{J}^{(2)}(\omega) \equiv dI/d\omega$, and the Inglis-Beliaev (IB) moment of inertia

$$\mathcal{J}_{IB}(\omega) = 2 \sum_{i>j} \frac{|J_{ij}(\omega)|^2}{\epsilon_i(\omega) + \epsilon_j(\omega)}, \quad (12)$$

which is the leading order term of the nuclear moment of inertia. Here $J_{ij}(\omega)$ is a matrix element of the angular momentum operator \hat{J}_z

$$J_{ij}(\omega) = \langle \phi(\omega) | [\hat{\alpha}_j \hat{\alpha}_i, \hat{J}_z] | \phi(\omega) \rangle. \quad (13)$$

It is well known [34] that the IB moment of inertia is too small to reproduce the absolute value of the moment of inertia. Comparing $\mathcal{J}_{IB}(\omega)$ and $\mathcal{J}^{(1)}(\omega)$ or $\mathcal{J}^{(2)}(\omega)$, we can find the validity of

¹From these β_{31} and β_{33} values, for an example, we can obtain the value of β_{30} for the x -quantization axis as

$$\beta_{30}^x = \frac{\sqrt{6}}{4} \beta_{31} - \frac{\sqrt{10}}{4} \beta_{33}. \quad (11)$$

using the $\mathcal{J}_{\text{IB}}(\omega)$ for the analysis of structural changes in the nuclear mean field. In addition, we analyze different contributions to the IB moment of inertia, Eq.(12),

$$\mathcal{J}_{\text{IB}}(\omega) = \sum_{\tau,s} \mathcal{J}_{\tau,s}(\omega) \equiv \mathcal{J}_{p,+1}(\omega) + \mathcal{J}_{p,-1}(\omega) + \mathcal{J}_{n,+1}(\omega) + \mathcal{J}_{n,-1}(\omega), \quad (14)$$

where (τ, s) denote the isospin $\tau = p, n$ and the z -simplex quantum number $s = \pm 1$ which characterize different subspaces. The comparison of different components of $\mathcal{J}_{\text{IB}}(\omega)$ could provide the information in which subspace the q.p. degrees of freedom mainly affect the bulk properties of the nuclei.

The cranking HFB equations (1a) are solved in an iterative way. As the convergence condition for each HFB state, we impose the condition

$$\sum_i \left| \epsilon_i^{(n)}(\omega) - \epsilon_i^{(n-1)}(\omega) \right| \leq .1[\text{KeV}], \quad (15)$$

where n is the number of iterations in the course of solving the cranking HFB equations.

3 Discussion of results

3.1 ^{32}S

In Figs.1-3 results for the yrast line states, angular momenta and deformations as functions of the rotational frequency are presented. The binding energy of the ground state in ^{32}S is well reproduced in our calculations (Fig.1). We found that the contribution from the pairing interaction terms to the total binding energy is almost negligible. The energy gaps between q.p. energies near the Fermi energies are large, about 4 MeV, both in the proton and neutron fields. Therefore, the calculations for the ND and SD bands have been done using the cranking HF approximation with the same parameter set as for the HFB calculations. While there are differences in details between our calculations and those with Skyrme forces [16], we obtained similar main results for the ND and SD bands. The SD band becomes the yrast one for $I \geq 12\hbar$. The excitation energy of the SD minimum relative to the ground state is about 10 MeV (Fig. 1). Except for the binding energy, these results are also consistent with those of SLy4-HF calculations [37], in which β -deformations are $\beta = .16$ and $\beta = .7$ in the ground state and SD minimum state, respectively. In comparison with the results of the Skyrme III calculations [16], however, finite values of the non-axial octupole deformation Y_{31} in the ND yrast band are obtained at larger rotational frequency $\omega \geq 1.5$ [MeV/ \hbar]. As is seen in Fig.4(a), the value of the non-axial octupole deformation $|\beta_{31}|$ increases suddenly at $\omega \sim 1.5$ [MeV/ \hbar], where the pseudo level-crossing occurs between s.p. orbits in the subspaces with $s = \pm 1$ (Fig.5(a)), both in the proton and neutron fields. These orbits can be associated with the principal quantum numbers $N = 2$ and $N = 3$ at $\omega = 0$ [MeV/ \hbar]. As a result, the Y_{31} deformation becomes favorable at $\omega \sim 2.2$ [MeV/ \hbar], for ^{32}S with a finite value $\beta_{31} = .13$. The density distribution projected on the plane perpendicular to the rotation axis is shown on Fig.6(a) for the octupole band at $\omega \sim 2.2$ [MeV/ \hbar] where the β_{31} deformation has a maximal value. High resolution γ - spectroscopy could test the validity of different predictions based on different nuclear interactions.

From the analysis of Figs.4(a), 7(a) it follows that there is a correlation between the behavior of the dynamical moment of inertia $\mathcal{J}^{(2)}(\omega)$ and the occurrence of the octupole deformation. Similar to the behavior of the $|\beta_{31}|$, the dynamical moment of inertia $\mathcal{J}^{(2)}(\omega)$ begins to increase at $\omega \sim 1.5$ [MeV/ \hbar], and both quantities show local maxima around $\omega \sim 2$ [MeV/ \hbar]. Due

to the strong octupole interaction the quasi-crossing between s.p. levels is smooth (Fig.5(a)). The static moment of inertia $\mathcal{J}^{(1)}(\omega)$ is less sensitive to the quasi-crossing of s.p. levels, and it changes smoothly with the increase of the rotational frequency ω . However, the IB moment of inertia may reflect the structural changes in a mean field like the dynamical moment of inertia $\mathcal{J}^{(2)}(\omega)$. In fact, it also begins to increase at $\omega \sim 1.5$ [MeV/ \hbar] and shows a local maximum at $\omega \sim 2.2$ [MeV/ \hbar]. The correlation between the IB moment of inertia and the magnitude of the octupole deformation $|\beta_{31}|$ may be understood within a simple two-level model presented in the Appendix A. According to this model, the two rotation-aligned single-particle states with a strong octupole coupling near the Fermi-surface may give a large contribution to the value of the IB moment of inertia. From Fig.8(a) follows that the magnitudes of $\mathcal{J}_{p,+1}(\omega)$ and $\mathcal{J}_{n,+1}(\omega)$ (see Eq.(14)) are smaller than those from the $s = -1$ subspaces which play the dominant roles in the collective rotation at low spins, in the region $\omega < 1.5$ [MeV/ \hbar]. However, at the $\omega > 1.5$ [MeV/ \hbar], $\mathcal{J}_{p,+1}(\omega)$ and $\mathcal{J}_{n,+1}(\omega)$ begin to increase rapidly, and they show local maxima at $\omega \sim 2.2$ [MeV/ \hbar] where $|\beta_{31}|$ also shows the maximum. Since $\mathcal{J}_{p,-1}(\omega)$ and $\mathcal{J}_{n,-1}(\omega)$ are almost unchanged in this region, the occurrence of the Y_{31} deformation is mainly due to the s.p. quasi-crossing in the $s = +1$ subspaces. To justify this statement we calculate the quantity $\cos^2 \psi(\omega)$ (see Appendix). Using the identity of the intruder orbits μ which have odd parity at $\omega = 0$ [MeV/ \hbar], we evaluate the $\cos^2 \psi(\omega)$ approximately as:

$$\cos^2 \psi(\omega) \approx \sum_{n_x+n_y+n_z=\text{odd}} |\langle n_x, n_y, n_z; \sigma | \mu(\omega) \rangle|^2, \quad (16)$$

where a s.p. vector $|n_x, n_y, n_z; \sigma\rangle$ is a component of the Goodman basis in the $s = +1$ subspace, and n_x , n_y and n_z are the number of quanta on the x -, y - and z - axes, respectively. As is shown in Fig.9(a), the evaluated value of $\cos^2 \psi(\omega) = 1/2$ or equivalently $|\psi(\omega)| = \pi/4$ at $\omega \sim 2.2$ [MeV/ \hbar]. According to the analysis within the two-level model (see Appendix), at this value of $|\psi(\omega)|$ the mixing of s.p. states with opposite parities is the strongest one.

Similar to the results of [16], our calculations show rather shallow minima for the β_{31} deformation. In Fig.10(a) we present results for the fluctuations of octupole and quadrupole deformations

$$\Delta Q_{lm} \equiv \frac{\sqrt{\langle \phi(\omega) | \hat{Q}_{lm}^2 | \phi(\omega) \rangle - \langle \phi(\omega) | \hat{Q}_{lm} | \phi(\omega) \rangle^2}}{|\langle \phi(\omega) | \hat{Q}_{lm} | \phi(\omega) \rangle|} \quad (17)$$

(see also Fig.11(a)). The contribution of the ground state octupole correlations may improve the mean field results. This contribution could be estimated, for example, in the random phase approximation like [38] according to the prescription [39], however, this is beyond the scope of the present paper.

As is seen in Fig.7(a), both moments of inertia, $\mathcal{J}^{(2)}(\omega)$ and $\mathcal{J}_{\text{IB}}(\omega)$, begin to increase again at $\omega \sim 2.5$ [MeV/ \hbar], which is apparently due to the quasi-crossings in the $s = -1$ subspaces at this point. There are also level-crossings between s.p. orbits with different simplex numbers (Fig.5(a)), which suggest the instability of the z -simplex symmetrized state at high spins. We may speculate that the breaking of the z -simplex symmetry due to the tilted or the chiral rotation [10] may lead to a better description of high spin states in ^{32}S at $\omega \geq 2.5$ [MeV/ \hbar].

3.2 ^{56}Ni

Our calculations reproduce the binding energies and the charge radii of ground states in $^{56-60}\text{Ni}$ quite well (Fig. 12). In this chain of nuclei we concentrate our attention on ^{56}Ni .

Though the shape of the ground state in ^{56}Ni is spherical, we also found two shape isomers with the ND and SD configuration at $\omega = 0$ [MeV/ \hbar], which are ~ 5 MeV and ~ 18 MeV

above the ground state, respectively (see Fig.13). The yrast non-rotating states observed in ^{56}Ni are related to vibrational excitations. In fact, their properties can be studied within the self-consistent cranking approach with the rotation *around a symmetry axis* [44] and we will discuss this subject in a forthcoming paper. The calculations for the ground state, ND and SD bands have been done in a similar manner to those of ^{32}S in the HF approximation, since the contribution of the pairing interaction terms to the total binding energies are almost negligible. On Fig.2 the evolution of the angular momentum with the increase of the rotational frequency is shown for SD and ND bands. At low spins the SD minimum is formed by the $4p-4h$ configuration with respect to the ground state in ^{56}Ni , $\pi[(3)^{-2}(4)^2]\nu[(3)^{-2}(4)^2]$, which has a prolate shape with the quadrupole deformation $\beta = .6$ (Fig.3). This is also $4h$ configuration with respect to the SD state in ^{60}Zn due to the $N = 30$ SD gap in the Zn isotopes [45], which is also seen in Fig.14. The MMM calculations [46, 47] also predict the SD shape at large rotational frequencies. We restricted, however, our analysis of the SD band in the region of $\omega = 0.0 - 0.4[\text{MeV}/\hbar]$, since at larger rotational frequencies the contribution of higher shells ($N > 10$) becomes important.

Using the decomposition of the rational harmonic oscillator (RHO) into the isotropic ones, the relation between multi-clusters and mean field results has been discussed in [48]. For SD shapes in the RHO the one symmetric and one asymmetric combinations of spherical oscillators are expected (see also [12]). Within the RHO the SD states in ^{56}Ni correspond to the asymmetric combination of two spherical oscillators with magic numbers 40 and 16. The density distribution of the SD state (see Fig.15) does not show such a multi-cluster structure at $\omega = 0$ [MeV/ \hbar]. The possible reason is that our configuration space is too small. However, the SD minimum could be related to the resonance state in the $^{28}\text{Si}+^{28}\text{Si}$ collision at high excitation energy $E_{\text{CM}}^* = 65 - 70\text{MeV}$ and high angular momenta $I = 34 - 42\hbar$ reported in [49, 50, 51]. A thorough study of ^{56}Ni as well as ^{32}S at high spins may help to understand the link between the tendency for nuclei to create strongly deformed shapes and the tendency to develop the cluster structure.

A prolate deformation $\beta = .35$ is found for the ND minimum (Fig. 3) at $\omega = 0.0$ [MeV/ \hbar]. With the increase of the rotational frequency the non-axial octupole deformation Y_{31} arises in the ND band. As is seen in Fig.4(b), the value of the non-axial octupole deformation increases rapidly around $\omega \sim .9[\text{MeV}/\hbar]$. It corresponds to $I \sim 10[\hbar]$, where the pseudo level-crossing occurs between s.p. orbits which have the principal quantum numbers $N = 3$ and $N = 4$, respectively, at $\omega = 0[\text{MeV}/\hbar]$ (Fig.5(b)). The maximal value of the Y_{31} deformation, $\beta_{31} = .09$, is approached at $\omega \sim 1.4[\text{MeV}/\hbar]$ (Fig.3(b)). As is seen in Fig. 8(b), $\mathcal{J}_{p,+1}(\omega)$ and $\mathcal{J}_{n,+1}(\omega)$ increase rapidly around $\omega \sim .9[\text{MeV}/\hbar]$ and approach the maximal value at $\omega \sim 1.3[\text{MeV}/\hbar]$. Using the two-level model and similar arguments as for the case of ^{32}S we may conclude: since $\mathcal{J}_{p,-1}(\omega)$ and $\mathcal{J}_{n,-1}(\omega)$ are decreasing in this region of the rotational frequency, it is most likely that the octupole deformation is caused by the quasi-crossing of s.p. levels, which have different parities at $\omega = 0[\text{MeV}/\hbar]$, in the $s = +1$ subspaces. Both $\cos^2 \psi(\omega)$ of the intruder orbits with the positive parity at $\omega = 0[\text{MeV}/\hbar]$ in the proton and neutron fields,

$$\cos^2 \psi(\omega) \approx \sum_{n_x+n_y+n_z=\text{even}} |\langle n_x, n_y, n_z; \sigma | \mu(\omega) \rangle|^2, \quad (18)$$

have maximal values at $\omega \sim 1.3[\text{MeV}/\hbar]$ and $\omega \sim 1.35[\text{MeV}/\hbar]$, where the components of the IB moment of inertia, $\mathcal{J}_{p,s=+1}(\omega)$ and $\mathcal{J}_{n,s=+1}(\omega)$, show maxima, respectively (Fig. 9 (b)).

The dynamical and IB moments of inertia also increase at $\omega \sim .9$ [MeV/ \hbar] and show maxima around $\omega \sim 1.2$ [MeV/ \hbar] (Fig.7(b)). However, the behavior of the $\mathcal{J}^{(2)}(\omega)$ and $\mathcal{J}_{\text{IB}}(\omega)$ moment of inertia is less correlated at larger values of the rotational frequency. The pseudo-crossing is much sharper in ^{56}Ni in comparison with the one in ^{32}S (Fig.5), i.e. the octupole interaction

is expected to be weaker. Both $\cos^2 \psi(\omega)$ decrease rapidly at $\omega > 1.55[\text{MeV}/\hbar]$ (see Fig.(9(b))). Due to the termination of the parity mixing of the s.p. levels, the matrix element $J_{ij}(\omega)$ between mixed states, Eq.(13), becomes rapidly small. As a result, the IB moment of inertia, $\mathcal{J}_{\text{IB}}(\omega)$, also decreases. On the other hand, the dynamical moment of inertia, $\mathcal{J}^{(2)}(\omega)$, reflects changes of the self-consistent mean field and, in particular, the modification of the two-body interaction due to the rotation. Due to the two-body interaction, the high intruder unoccupied state ($s = +$) contributes to the sudden increase of the dynamical moment of inertia observed at high rotational frequencies $\omega > 1.5[\text{MeV}/\hbar]$.

The fluctuations of octupole deformations ΔQ_{31} and ΔQ_{33} are always larger than 1 in all region of the ND band (Fig. 10(b)), in spite of the presence of the octupole minimum (Fig. 11(b)). The octupole minimum in ^{56}Ni is much more shallow in comparison with the one of ^{32}S and it could explain large fluctuations of the octupole deformations in the considered case.

4 Summary

It was expected from various calculations based on the MMM that octupole deformations would arise in rotating nuclei [3]. Using the cranking HF(B) approach with the effective Gogny interaction, we found that the non-axial octupole deformation associated with the Y_{31} term in the octupole family becomes important in the yrast band of ^{32}S at the angular momenta $I \geq 5[\hbar]$. The primary mechanism behind the occurrence of the octupole deformation is related to the strong mixing via octupole interaction of s.p. orbits with a positive simplex quantum number. Similar phenomena have been observed in the nucleus ^{56}Ni , where we predict the octupole softness in the excited ND band at high spins $I \geq 10[\hbar]$.

Finally, an exploration of the octupole phenomenon certainly could deepen our understanding of different aspects of a spontaneous symmetry breaking mechanism in finite Fermi systems like nuclei. In particular, the breaking of the intrinsic reflection symmetry could be related to unexpected strong electric dipole and octupole transitions in rotational bands and to a formation of multi-cluster structures in strongly deformed nuclei. Measurements using new generations of modern detectors can test the predictions made within the HF(B) approach and lead to new insights regarding effective nucleon-nucleon interactions and their properties.

Acknowledgements

We are thankful to F. Sakata, Y. Hashimoto and Y. Kanada-En'yo for their support in numerical calculations. We are also grateful to K. Matsuyanagi for illuminating communications. This work was supported in part by the RFFI under Grant 00-02-17194.

A A two-level model

Let us consider the situation such that the high-lying intruder s.p. orbit μ is coming down to the highest-lying occupied orbit ν due to the Coriolis term $-\omega \hat{J}_z$; they have the same simplex quantum number. For the sake of simplicity, we restrict our discussion within the 2×2 subspace. We assume that i) our states are eigenstates of the parity operator P at $\omega = 0$; ii) there are no changes in the subspace expanded by the simplex partners of μ and ν at $\omega \neq 0$.

At $0 \leq \omega \leq \omega_c$ the eigenstates can be written as

$$|\nu(\omega)\rangle = \cos \psi(\omega)|\nu(\omega = 0)\rangle + \sin \psi(\omega)|\mu(\omega = 0)\rangle,$$

$$|\mu(\omega)\rangle = \cos \psi(\omega)|\mu(\omega=0)\rangle - \sin \psi(\omega)|\nu(\omega=0)\rangle, \quad (\text{A.1})$$

where $|\psi(\omega)|$ is a monotonic function of ω ², which satisfies the following conditions;

$$0 \leq |\psi(\omega)| \leq \frac{\pi}{2}, \quad (\text{A.2})$$

$$\psi(\omega=0) = 0, \quad |\psi(\omega_c)| = \frac{\pi}{2}.$$

Here, ω_c is the largest rotational frequency. Using the unitary transformation in Eq.(A.1), at $\omega \neq 0$ the density matrix has the following form in this subspace

$$\begin{aligned} \boldsymbol{\rho}(\omega) &\equiv \begin{pmatrix} \rho_{\nu\nu}(\omega) & \rho_{\nu\mu}(\omega) \\ \rho_{\mu\nu}(\omega) & \rho_{\mu\mu}(\omega) \end{pmatrix} \\ &= \begin{pmatrix} \cos \psi(\omega) & \sin \psi(\omega) \\ -\sin \psi(\omega) & \cos \psi(\omega) \end{pmatrix} \cdot \begin{pmatrix} 1 & 0 \\ 0 & 0 \end{pmatrix} \\ &\quad \cdot \begin{pmatrix} \cos \psi(\omega) & -\sin \psi(\omega) \\ \sin \psi(\omega) & \cos \psi(\omega) \end{pmatrix} \\ &= \begin{pmatrix} \cos^2 \psi(\omega) & -\sin 2\psi(\omega)/2 \\ -\sin 2\psi(\omega)/2 & \sin^2 \psi(\omega) \end{pmatrix}. \end{aligned} \quad (\text{A.3})$$

At $\omega = 0$, the matrix elements of the octupole operator \hat{Q}_3 have the following structure

$$\mathbf{q} \equiv \begin{pmatrix} q_{\nu\nu} & q_{\nu\mu} \\ q_{\mu\nu} & q_{\mu\mu} \end{pmatrix} = \begin{pmatrix} 0 & q \\ q & 0 \end{pmatrix}, \quad (\text{A.4})$$

where q is a finite real number. At $\omega \neq 0$ the expectation value of \hat{Q}_3 is

$$|\langle \hat{Q}_3 \rangle| = |\text{tr}(\mathbf{q}\boldsymbol{\rho}(\omega))| = |q \sin 2\psi(\omega)|, \quad (\text{A.5})$$

due to the assumption ii).

At $\omega = 0$ matrix elements of the angular momentum operator \hat{J}_z are defined as

$$\mathbf{j} \equiv \begin{pmatrix} j_{\nu\nu} & j_{\nu\mu} \\ j_{\mu\nu} & j_{\mu\mu} \end{pmatrix} = \begin{pmatrix} j & 0 \\ 0 & j' \end{pmatrix}. \quad (\text{A.6})$$

At $\omega \neq 0$, using the unitary transformation in Eq.(A.1), we obtain for the matrix elements of \mathbf{j}

$$\begin{aligned} \begin{pmatrix} j_{\nu\nu}(\omega) & j_{\nu\mu}(\omega) \\ j_{\mu\nu}(\omega) & j_{\mu\mu}(\omega) \end{pmatrix} &= \\ \begin{pmatrix} j \cos^2 \psi(\omega) + j' \sin^2 \psi(\omega) & (j' - j) \sin 2\psi(\omega)/2 \\ (j' - j) \sin 2\psi(\omega)/2 & j' \cos^2 \psi(\omega) + j \sin^2 \psi(\omega) \end{pmatrix}, \end{aligned} \quad (\text{A.7})$$

From Eqs. (A.5) and (A.7), it follows that $|\langle \hat{Q}_3 \rangle|$ and $|j_{\mu\nu}(\omega)|^2 = (j' - j)^2 \sin^2 2\psi(\omega)/4$ have a maximum at $|\psi(\omega)| = \pi/4$, where there is a strong mixing of the unperturbed eigenfunctions. Therefore, the $\mu\nu$ component of the Inglis-Beliaev moment of inertia

$$\frac{2|j_{\mu\nu}(\omega)|^2}{\epsilon_\mu(\omega) + \epsilon_\nu(\omega)} = \frac{(j' - j)^2 \sin^2 2\psi(\omega)}{2(\epsilon_\mu(\omega) + \epsilon_\nu(\omega))} \quad (\text{A.8})$$

can be large enough to affect the total value of the moment of inertia due to the smallness of its denominator $\epsilon_\mu(\omega) + \epsilon_\nu(\omega)$ at this rotational frequency.

²A sign of $\psi(\omega)$ is not important for the absolute value of the octupole deformation.

References

- [1] A. Bohr and B. Mottelson, *Nuclear Structure*, Vol.2 (Benjamin, New York, 1975)
- [2] P. Ring and P.Schuck, *The Nuclear Many-Body Problem* (Springer-Verlag, Berlin, 1980)
- [3] S. Åberg, H. Flocard and W. Nazarewicz, *Annu. Rev. Nucl. Part. Sci.* **40**, 439 (1990).
- [4] Z. Patyk, A. Baran, J.F. Berger, J. Dechargé, J. Dobaczewski, P. Ring and A. Sobiczewski, *Phys.Rev.* **C59**, 704 (1999).
- [5] P.J. Nolan and P.J. Twin, *Annu. Rev. Nucl.Part. Sci.* **38**, 533 (1988).
- [6] R.V.F. Janssens and T.L. Khoo, *Annu. Rev. Nucl.Part. Sci.* **41**, 321 (1991).
- [7] C. Baktash, B. Haas and W. Nazarewicz, *Annu. Rev. Nucl.Part. Sci.* **45**, 485 (1995).
- [8] C. Baktash, *Prog. Part. Nucl. Phys.* **38**, 291 (1997).
- [9] P.A. Butler and W. Nazarewicz, *Rev. Mod. Phys.* **68**, 350 (1996).
- [10] S. Frauendorf, submitted to *Rev. Mod. Phys.*
- [11] T.Nakatsukasa, K.Matsuyanagi and S.Mizutori, *Progr. Theor. Phys.* **87**, 607 (1992).
- [12] R. Nazmitdinov and S. Åberg, *Phys.Lett.* **B289**, 238 (1992).
- [13] R.R. Chasman, *Phys.Lett.* **B266**, 243 (1991).
- [14] X. Li and J. Dudek, *Phys.Rev.* **C49**, R1250 (1994).
- [15] S. Takami, K. Yabana and M. Matsuo, *Phys. Lett.* **B341**, 242 (1998).
- [16] M. Yamagami and K. Matsuyanagi, *Proc. Int. Conf. on Nuclear Structure '98*, edited by C. Baktash (Gatlinburg, Tennessee, 1998), p.327; nucl-th/9908060.
- [17] W. D. Heiss, R. G. Nazmitdinov and S. Radu, *Phys. Rev. Lett.* **72**, 2351 (1994); *Phys. Rev.* **B51**, 1874 (1994); *Phys. Rev.* **C52**, 3032 (1995).
- [18] A. Arita and K. Matsuyanagi, *Progr. Theor. Phys.* **91**, 723 (1994); *Nucl. Phys.* **A592**, 9 (1995).
- [19] W. D. Heiss, R. A. Lynch and R. G. Nazmitdinov, *JETP Lett.* **69**, 563 (1998).
- [20] W. D. Heiss, R. A. Lynch and R. G. Nazmitdinov, *Phys. Rev.* **C60**, 034303 (1999).
- [21] D. Gogny, *Nuclear Self-consistent Fields*, edited by G. Ripka and M. Porneuf, (North-Holland, Amsterdam, 1973) p.333;
- [22] J. Dechargé and D. Gogny, *Phys. Rev.* **C21**, 1568 (1980).
- [23] M. Girod and B. Grammaticos, *Phys. Rev.* **C27**, 2317 (1983).
- [24] J. F. Berger, M. Girod and D. Gogny, *Nucl. Phys.* **A428**, 23c (1984); *Nucl. Phys.* **A502**, 85c (1989); *Comp. Phys. Comm.* **63**, 365 (1991).

- [25] J. L. Egido and L. M. Robledo, Phys. Rev. Lett. **70**, 2876 (1993); J. L. Egido, L. M. Robledo and R. R. Chasman Phys. Lett. **B322**, 22 (1994).
- [26] M. Girod, J. P. Delaroche, J. F. Berger and J. Libert, Phys. Lett. **B325**, 1 (1994).
- [27] E. Caurier, J. L. Egido, G. Martínez-Pinedo, A. Poves, J. Retamosa, L. M. Robledo and A. P. Zuker, Phys. Rev. Lett. **75** 2466 (1995); G. Martínez-Pinedo, A. Poves, L. M. Robledo, E. Caurier, F. Nowacki, J. Retamosa, and A. P. Zuker, Phys. Rev. **C54**, R2154 (1996); S. M. Lenzi *et al.*, Phys. Rev. **C56**, 1313 (1997).
- [28] T. Tanaka, F. Sakata, and K. Iwasawa, Phys. Rev. **C58**, 2765 (1998).
- [29] T. Tanaka, F. Sakata, T. Marumori and K. Iwasawa, Phys. Rev. **C56**, 180 (1997).
- [30] K. Iwasawa, F. Sakata, T. Tanaka, Y. Hashimoto and T. Marumori, *Progress in Particle and Nuclear Physics* **38**, 249 (Elsevier Science, 1997).
- [31] J. Dobaczewski, J. Dudek, S. G. Rohozinski and T. R. Werner, nucl-th/9912072; nucl-th/9912073.
- [32] H. Flocard, P. Quentin, A. K. Kerman and D. Vautherin, Nucl. Phys. **A203**, 433 (1973).
- [33] A. L. Goodman, in *Advances in Nuclear Physics*, edited by J. W. Negele and E. Vogt (Plenum, New York, 1979), Vol. 11, p. 293.
- [34] D.J. Thouless and J.G. Valatin, Nucl.Phys. **31**, 211 (1962).
- [35] G. Audi and A. H. Wapstra, Nucl. Phys. **A565**, 1 (1993).
- [36] P. M. Endt, Nucl. Phys. **A521**, 1 (1990).
- [37] H. Molique, J. Dobaczewski and J. Dudek, nucl-th/9907103.
- [38] J. Kvasil and R.G. Nazmitdinov, Nucl. Phys. **A439**, 86 (1985)
- [39] F. Dönau, D. Almeded and R.G. Nazmitdinov, Phys.Rev.Lett. **83**, 280 (1999).
- [40] J. Dobaczewski, W. Nazarewicz and T. R. Werner, Z. Phys. **A354** 27 (1996).
- [41] E. G. Nadjakov, K. P. Marinova and Yu. P. Gangrsky, At. Nucl. D. Tab. , **56**, 133 (1994).
- [42] B. A. Nikolaus T. Hoch and D. G. Madland, Phys. Rev. **C46**, 1757 (1992).
- [43] H. Junde, Nuclear Data Sheets, **67**, 523 (1992).
- [44] E. R. Marshalek and R. G. Nazmitdinov, Phys. Lett. **B300**, 199 (1993); E. R. Marshalek, R. G. Nazmitdinov and I. Ragnarsson, Bulletin of Russian Academy of Sciences: Physics, **57**, 1709 (1993).
- [45] C. E. Svensson *et al.*, Phys. Rev. Lett. **79** 1233 (1997); Phys. Rev. Lett. **82** 3400 (1999); M. Devlin *et al.*, Phys. Rev. Lett. **82**, 1233 (1999).
- [46] R. K. Sheline, I. Ragnarsson and S. G. Nilsson, Phys. Lett. **B41**, 115 (1972).
- [47] T. Bengtsson, M. Faber, M. Ploszajczak, I. Ragnarsson and S. Åberg, Lund-MPh-84/01.

- [48] W. Nazarewicz and J. Dobaczewski, Phys. Rev. Lett. **68**, 154 (1992).
- [49] R. R. Betts et al., Phys. Rev. Lett. **47**, 23 (1981). R. R. Betts, Nucl. Phys. **A447**, 257c (1985).
- [50] E. Uegaki and Y. Abe, Phys. Lett. **B340**, 143 (1994).
- [51] R. Nouicer et al., Phys. Rev. **C60**, 041303(1999).

Figure Captions

Figure 1: The total binding energy in ^{32}S as a function of the angular momentum. The calculated points indicated by symbols '+' and 'x' for ND and SD states, respectively, are connected by solid lines. Experimental values for states with different parities and spins are indicated by symbols: filled square is used for the positive parity and even values of I ; open square is used for the negative parity and even values of I ; filled triangle is used for the positive parity and odd values of I ; inverse open triangle is used for the negative parity and odd values of I . The experimental values of the total binding energy and excited levels from Refs. [35] and [36], respectively.

Figure 2: The angular momentum I versus the rotational frequency ω in ^{32}S and ^{56}Ni . The calculated values of the angular momentum connected by solid lines are indicated by symbols: filled square and filled circle are used for ND and SD states, respectively, for ^{32}S ; open square and open circle are used for ND and SD states, respectively, for ^{56}Ni ; '+' and 'x' are used for the results of calculations with the Skyrme III interaction [16].

Figure 3: β -deformations in ^{32}S and ^{56}Ni as a function of the rotational frequency ω . The symbols are used here are defined in Fig.2

Figure 4: The non-axial octupole deformation: (a) in the ND yrast band of ^{32}S and (b) in the ND excited band of ^{56}Ni , – as a function of the rotational frequency ω . The calculated values connected by solid lines are indicated by symbols: filled square is used for $|\beta_{31}|$; open square is used for $|\beta_{33}|$. SIII means the results of Ref. [16].

Figure 5: Neutron single-particle energies near the Fermi surface versus the rotational frequency ω : (a) in ^{32}S and (b) in ^{56}Ni . The occupied states with different simplex quantum number s connected by lines are indicated by symbols: filled square and open square are used for the $s = +1$ and $s = -1$ states, respectively. The unoccupied states with the simplex $s = +1$ and $s = -1$ are connected by solid and dotted lines, respectively.

Figure 6: The density distribution: (a) in the ND yrast band of ^{32}S at $\omega = 2.2$ [MeV/ \hbar]; (b) in the ND excited band of ^{56}Ni at $\omega = 1.4$ [MeV/ \hbar].

Figure 7: The static, $\mathcal{J}^{(1)}(\omega)$, the dynamical, $\mathcal{J}^{(2)}(\omega)$, and the Inglis-Beliaev, $\mathcal{J}_{IB}(\omega)$, moments of inertia versus the rotational frequency ω : (a) in the ND yrast band in ^{32}S ; (b) in the ND excited band in ^{56}Ni . See the definition of different moments of inertia in the text.

Figure 8: Components of the Inglis-Beliaev, $\mathcal{J}_{IB}(\omega)$, moment of inertia as a function of the rotational frequency ω : (a) in ^{32}S and (b) in ^{56}Ni . Notations of components are defined in Eq. (14).

Figure 9: The degree of mixing of intruder orbits, $\cos^2 \psi(\omega)$, in the region of quasi-crossing: (a) in ^{32}S and (b) in ^{56}Ni . The quantity $\cos^2 \psi(\omega)$ is defined in the text.

Figure 10: The inverse of fluctuation of the octupole and quadrupole moments as a function of the rotational frequency ω : (a) in the ND yrast band in ^{32}S ; (b) in the ND excited band in ^{56}Ni . The fluctuation ΔQ_{lm} is defined by Eq.(17).

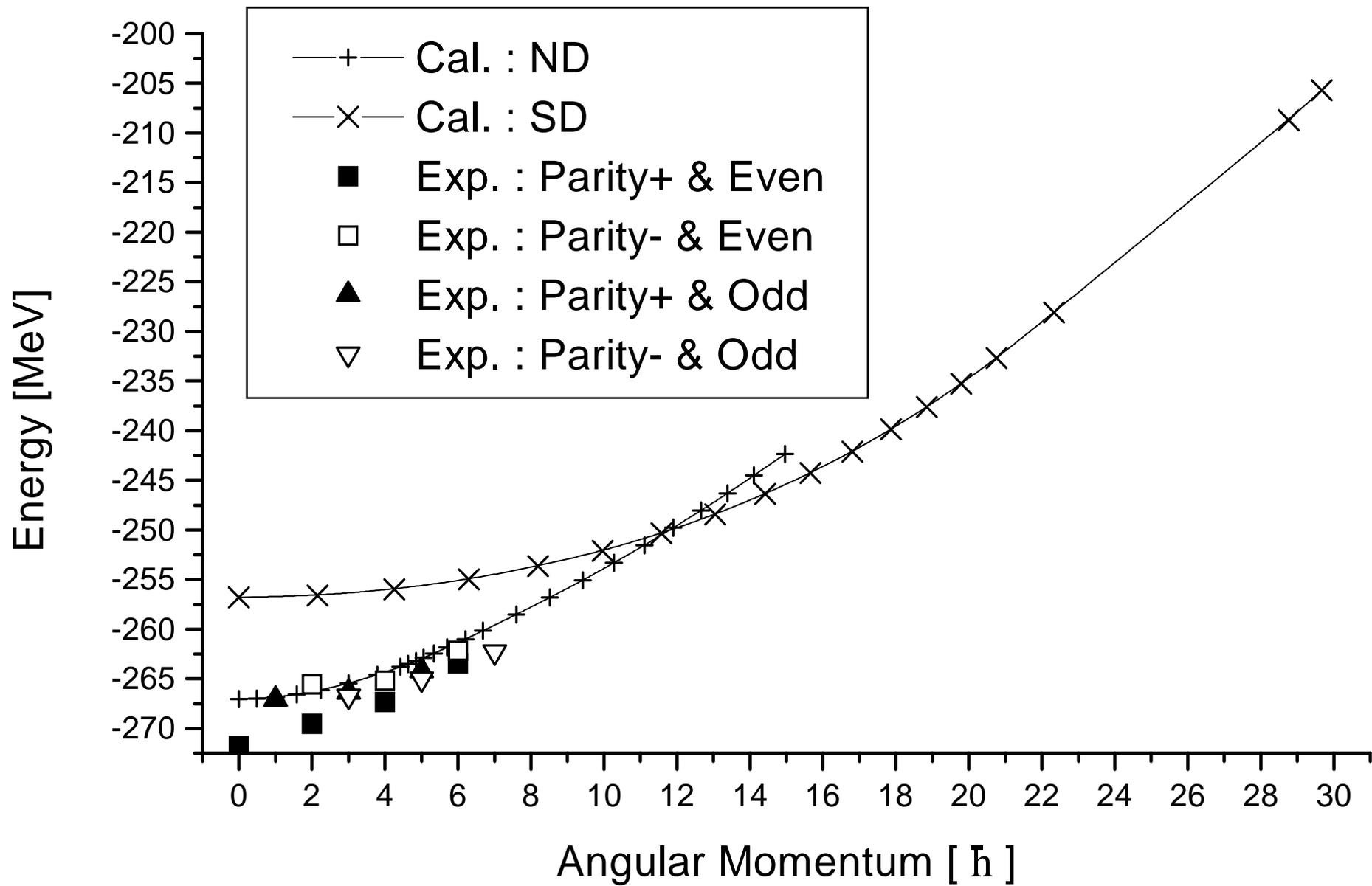
Figure 11: The potential energy curve along the β_{31} direction: (a) in ^{32}S and (b) in ^{56}Ni . The calculated values of the β_{31} indicated by symbols are connected by solid line.

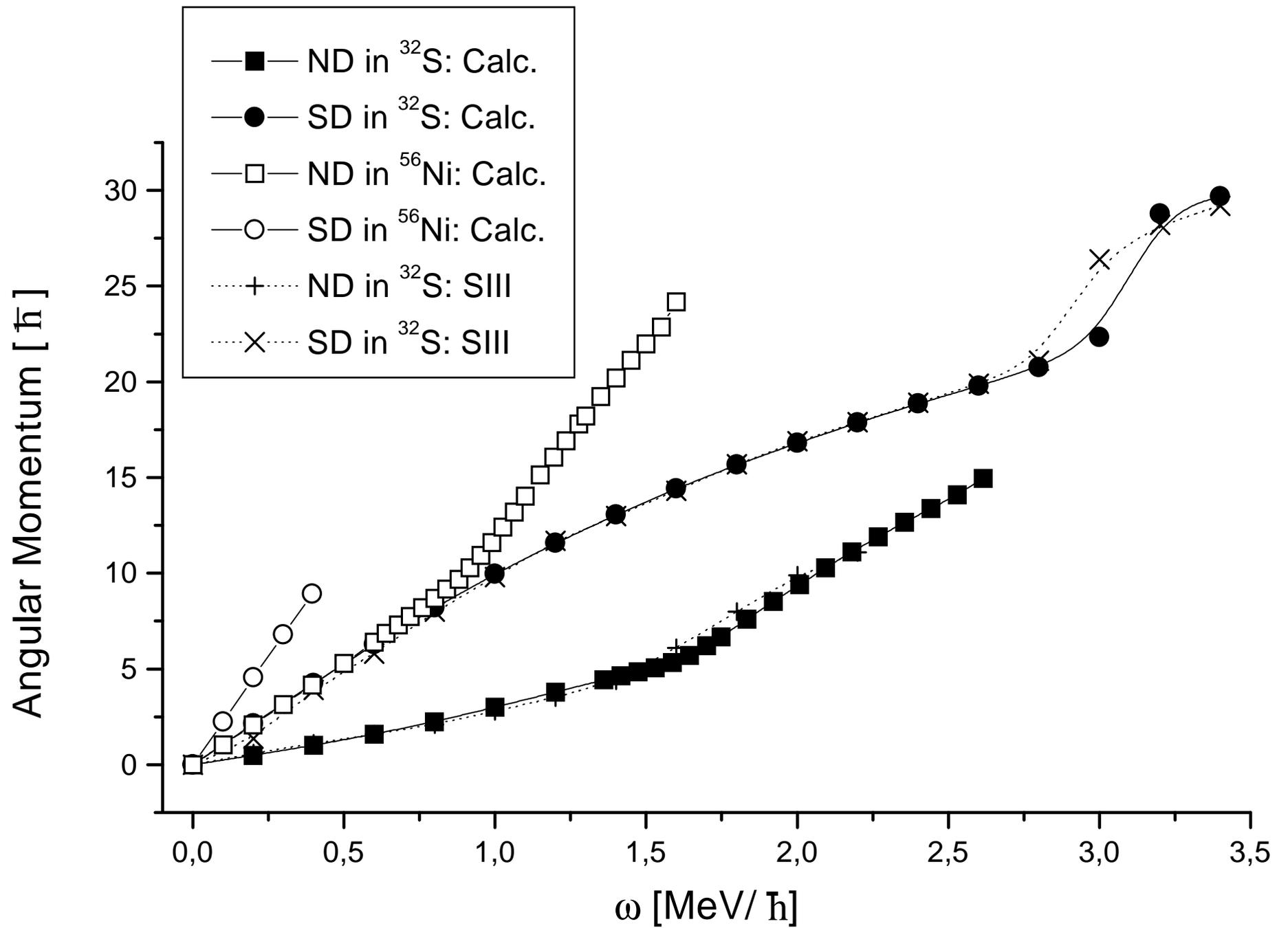
Figure 12: (a)The total binding energy and (b) the charge radius in nickel isotopes. Experimental values of total binding energies from Ref. [35]. A charge radius r_c is calculated with the approximation $r_c^2 = r_p^2 + .64$ [fm²] [40] from the calculated values of proton radius r_p . Experimental values of r_c for $^{58,60}Ni$ from Ref. [41]; for ^{56}Ni it is the extrapolated value from Ref. [42].

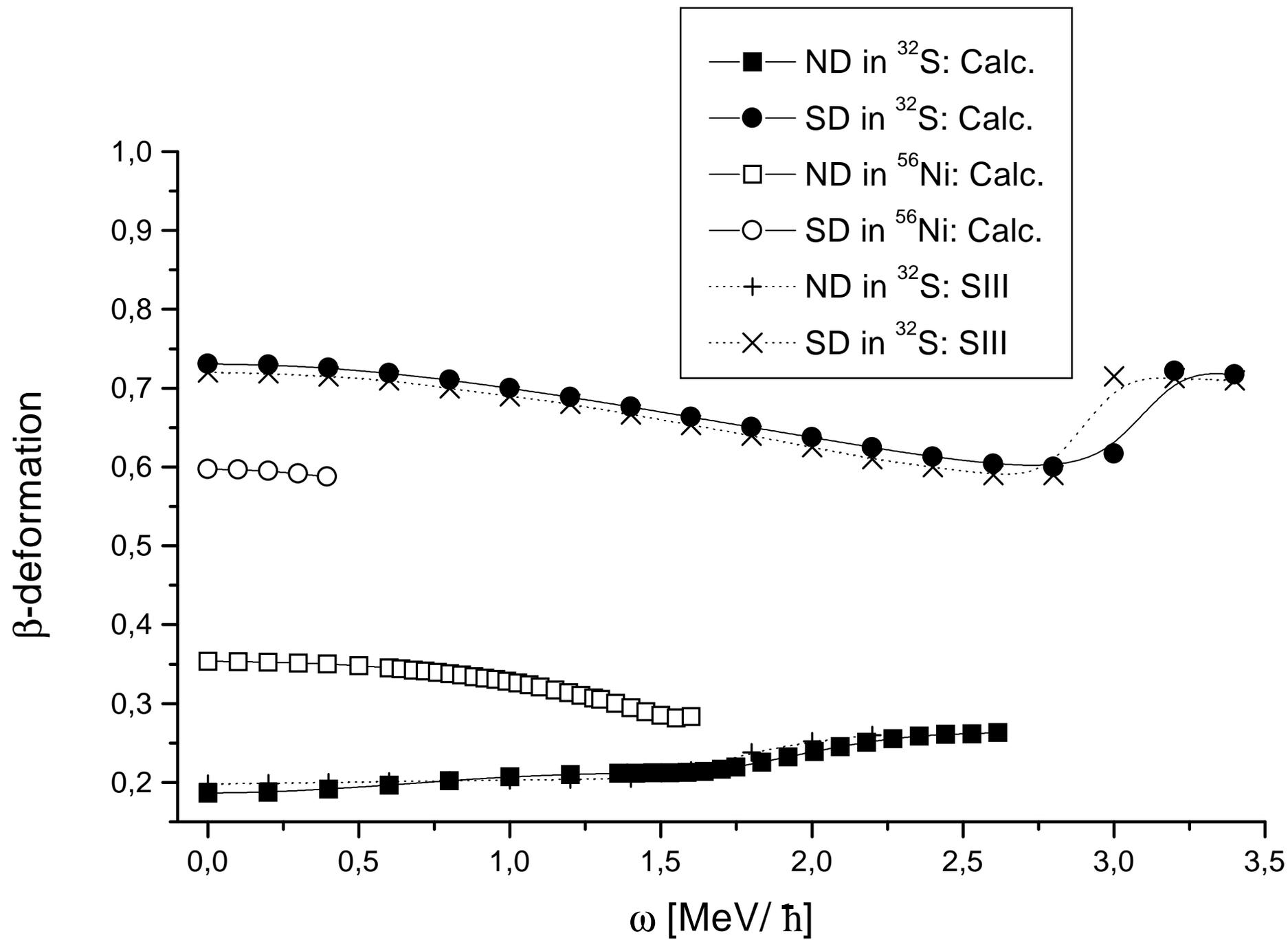
Figure 13: The total binding energy in ^{56}Ni as a function of the angular momentum. The calculated points indicated by symbols ‘+’ and ‘×’ for SD and ND states, respectively, are connected by solid lines. Experimental values for different states are indicated by symbols: filled square is used for yrast non-rotating states; open square is used for the excited states whose binding energies are proportional to $I(I+1)$ [\hbar^2] starting from the 0_3^+ state; filled circle is used for other states. The calculations of the ground spherical state reproduce the experimental ground binding energy quite well. Experimental values of the total binding energy and excited levels from Refs. [35] and [43], respectively.

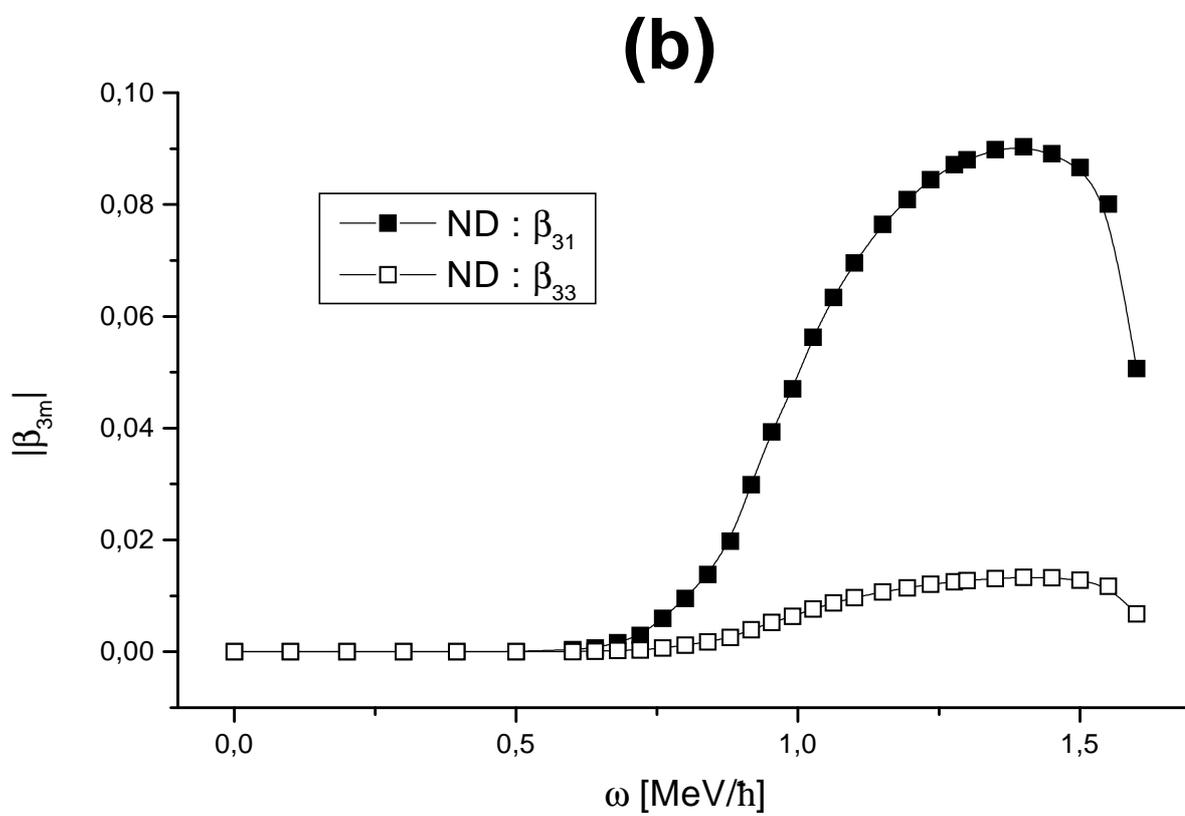
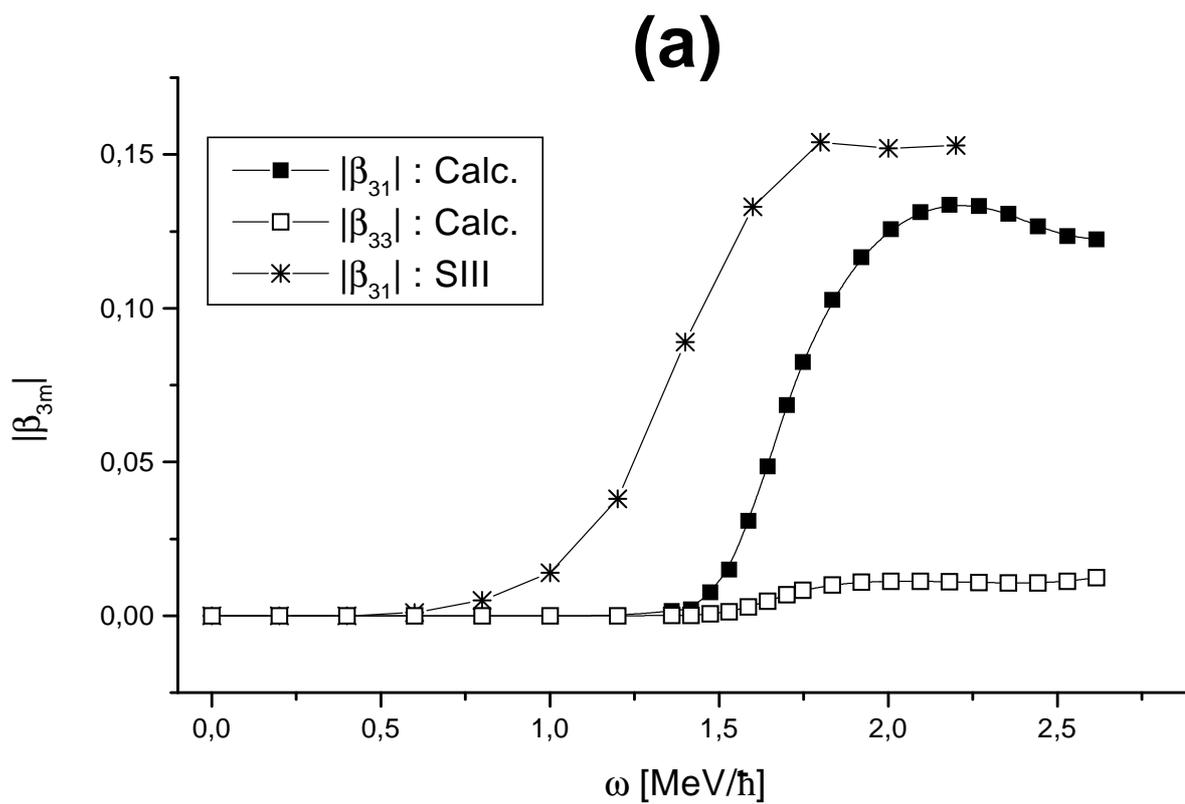
Figure 14: Neutron single-particle energies of ^{56}Ni along the SD band near the Fermi surface. The symbols are used here are defined in Fig.5.

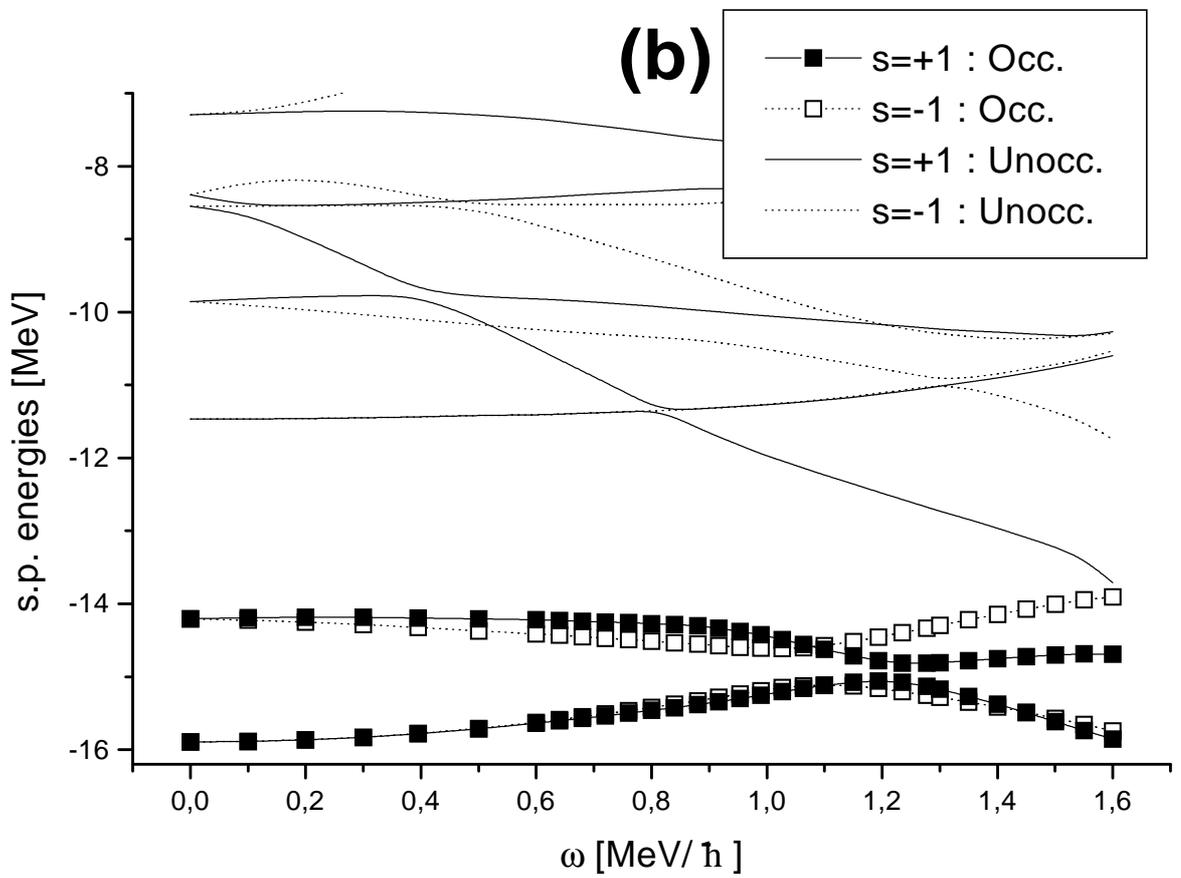
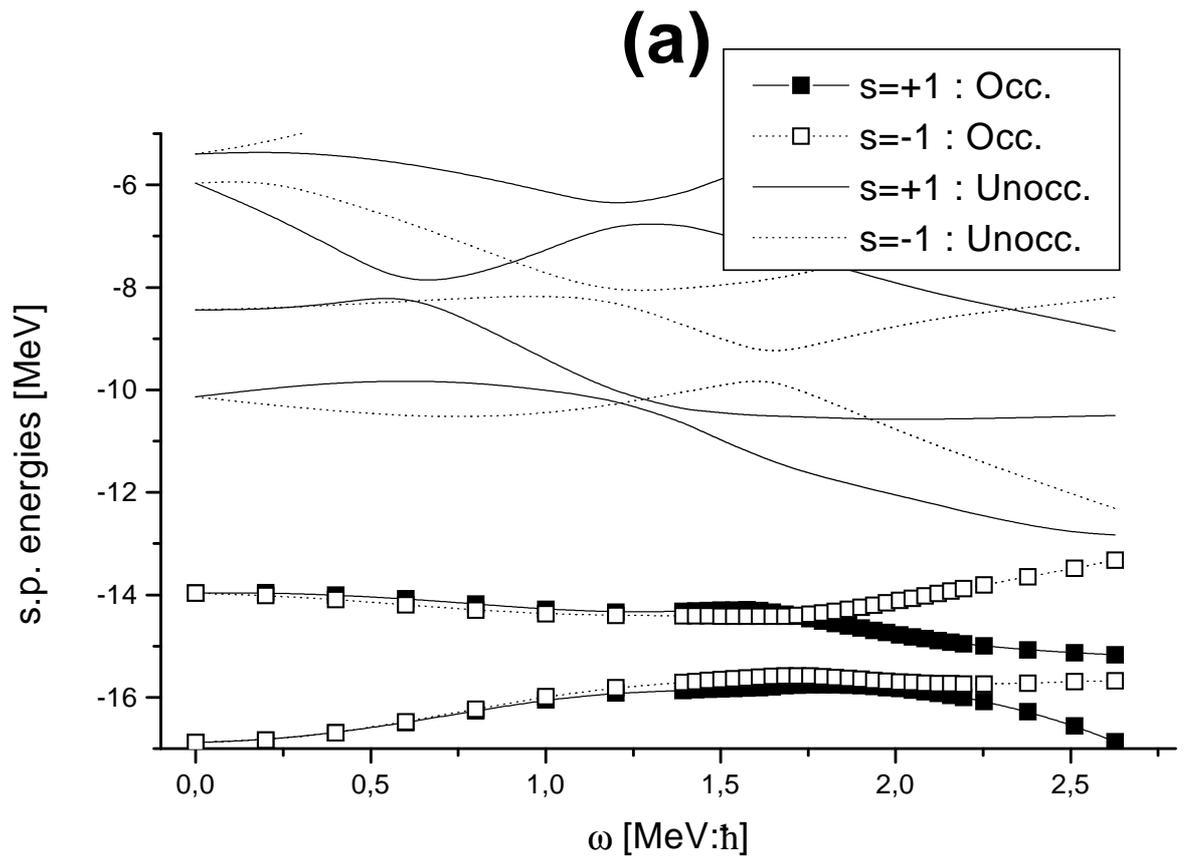
Figure 15: The density distribution of SD minimum at $\omega = 0$ [MeV/ \hbar] in ^{56}Ni .



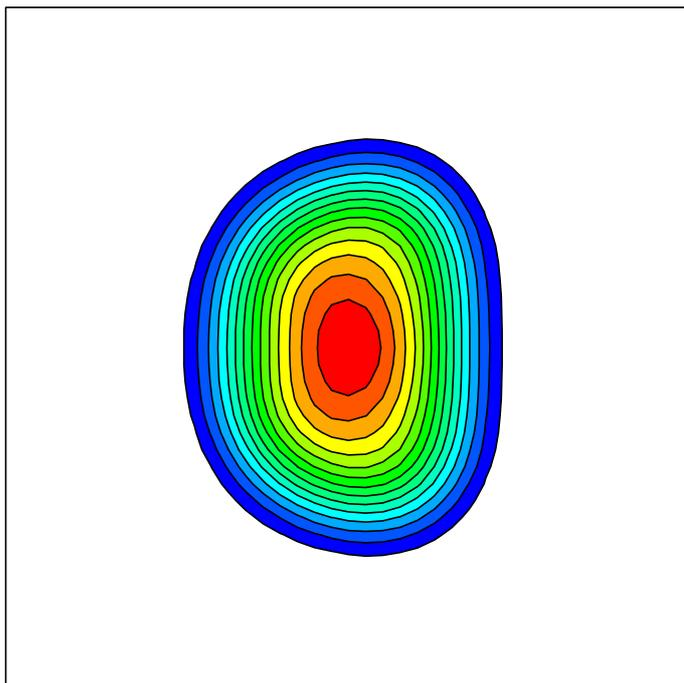




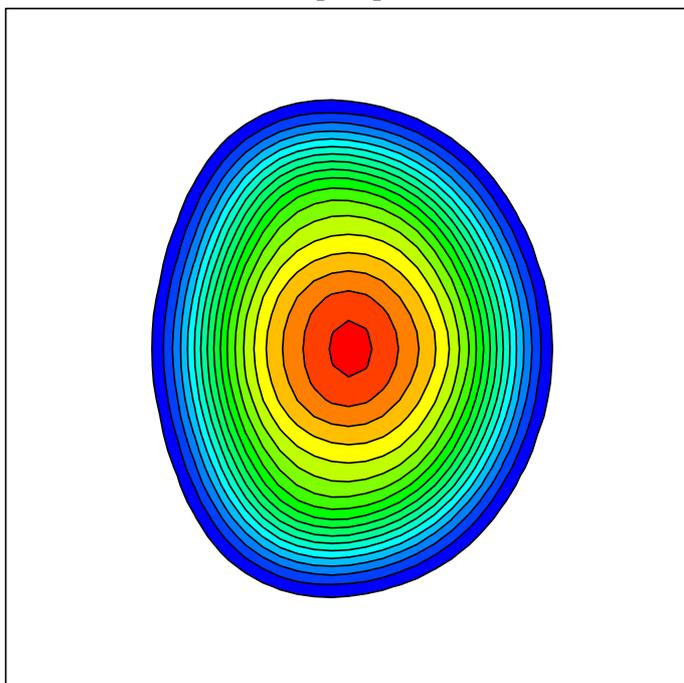


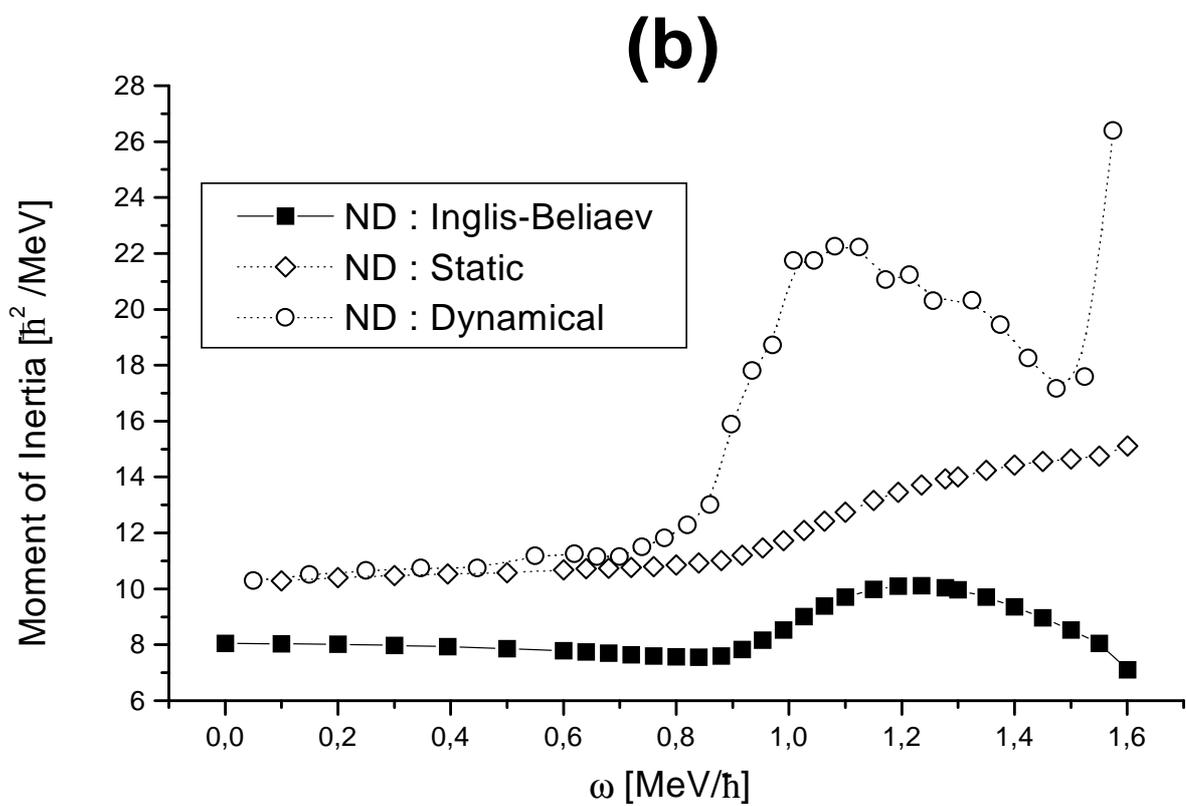
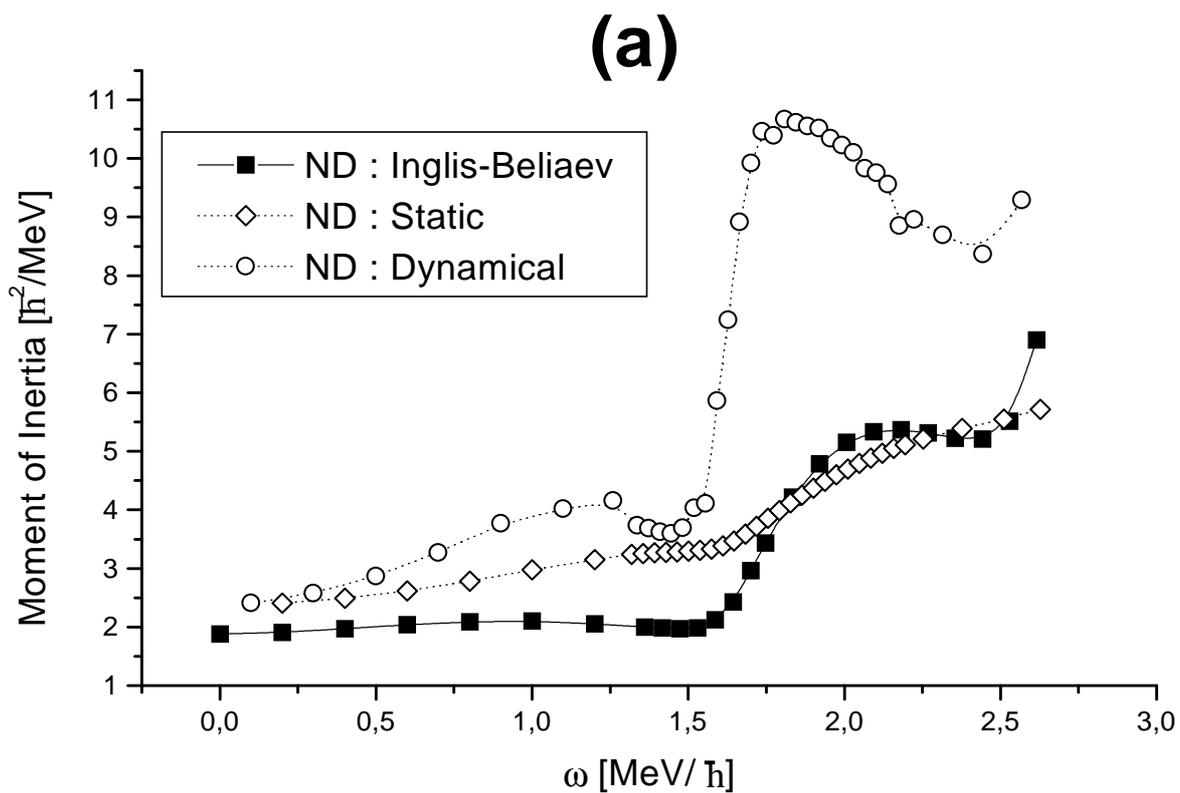


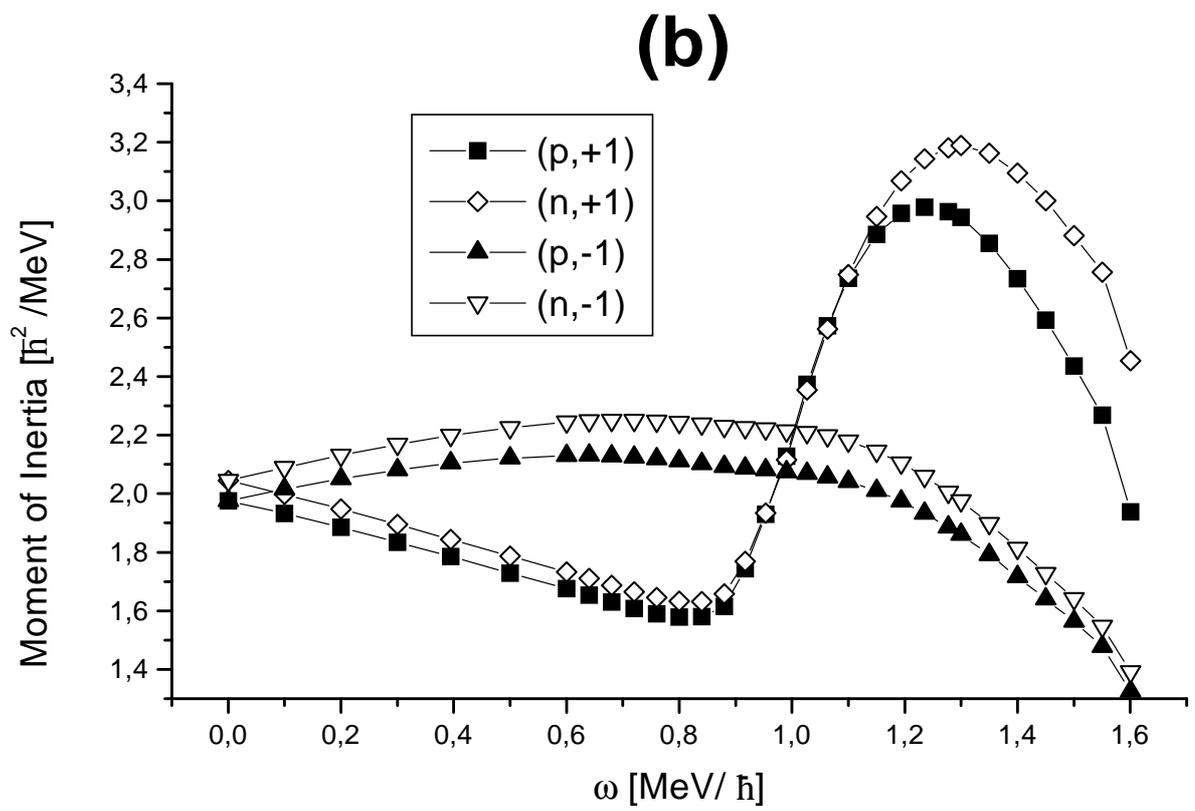
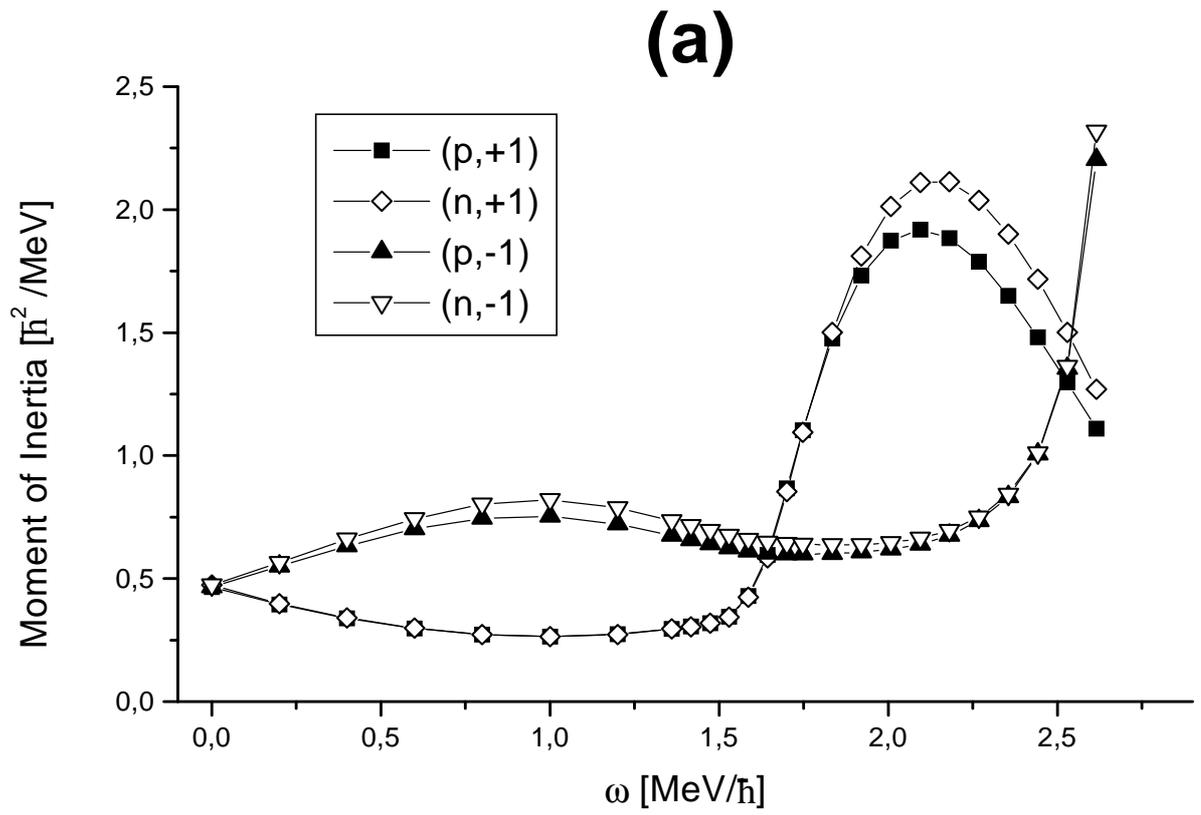
(a)



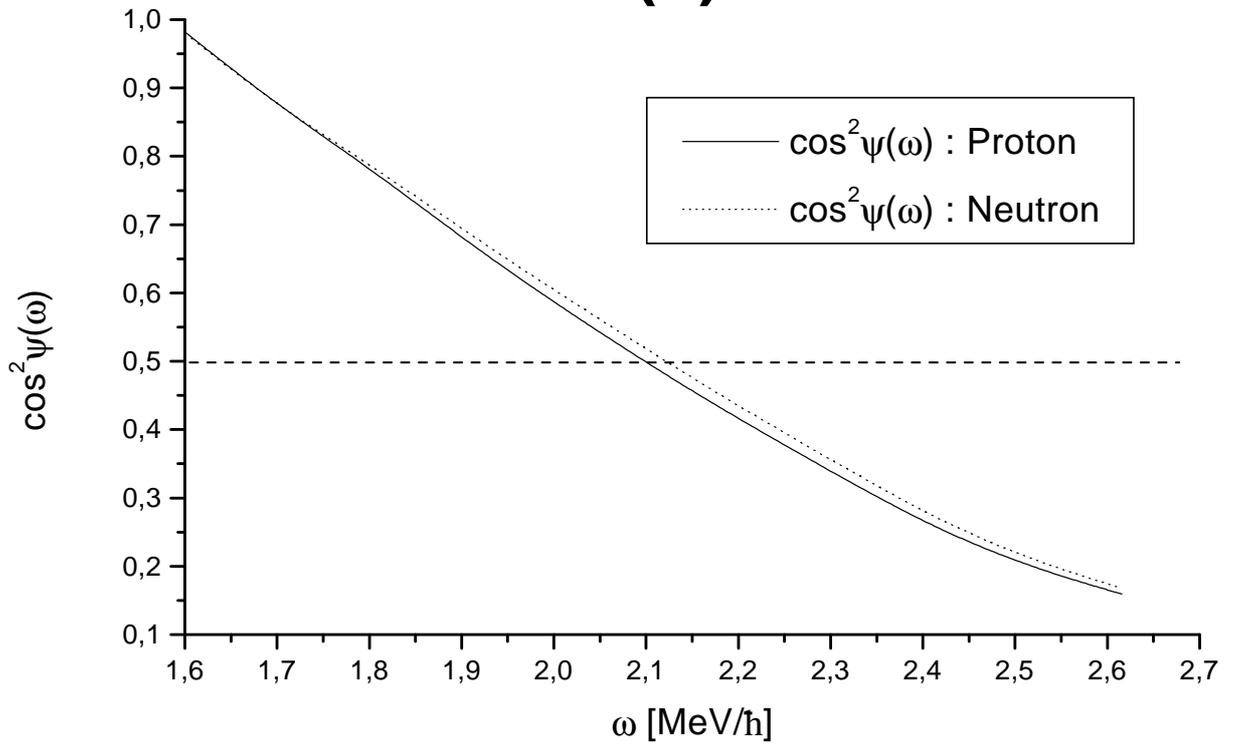
(b)



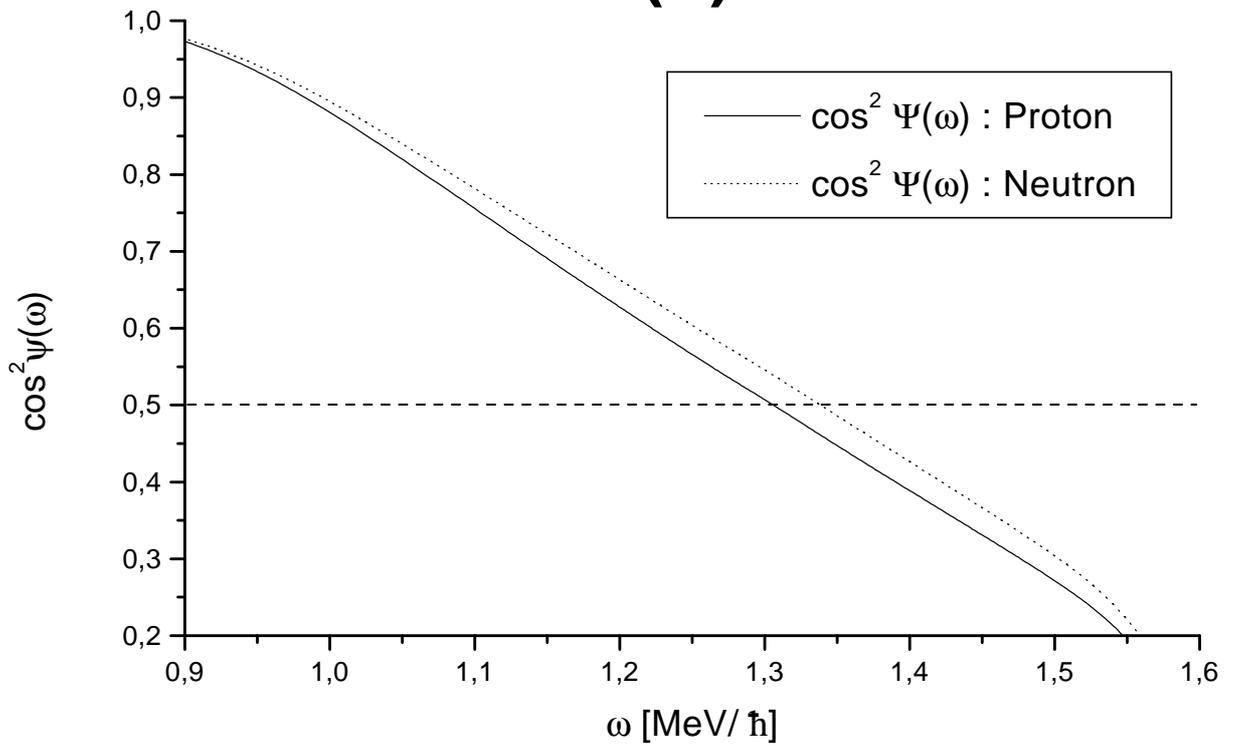


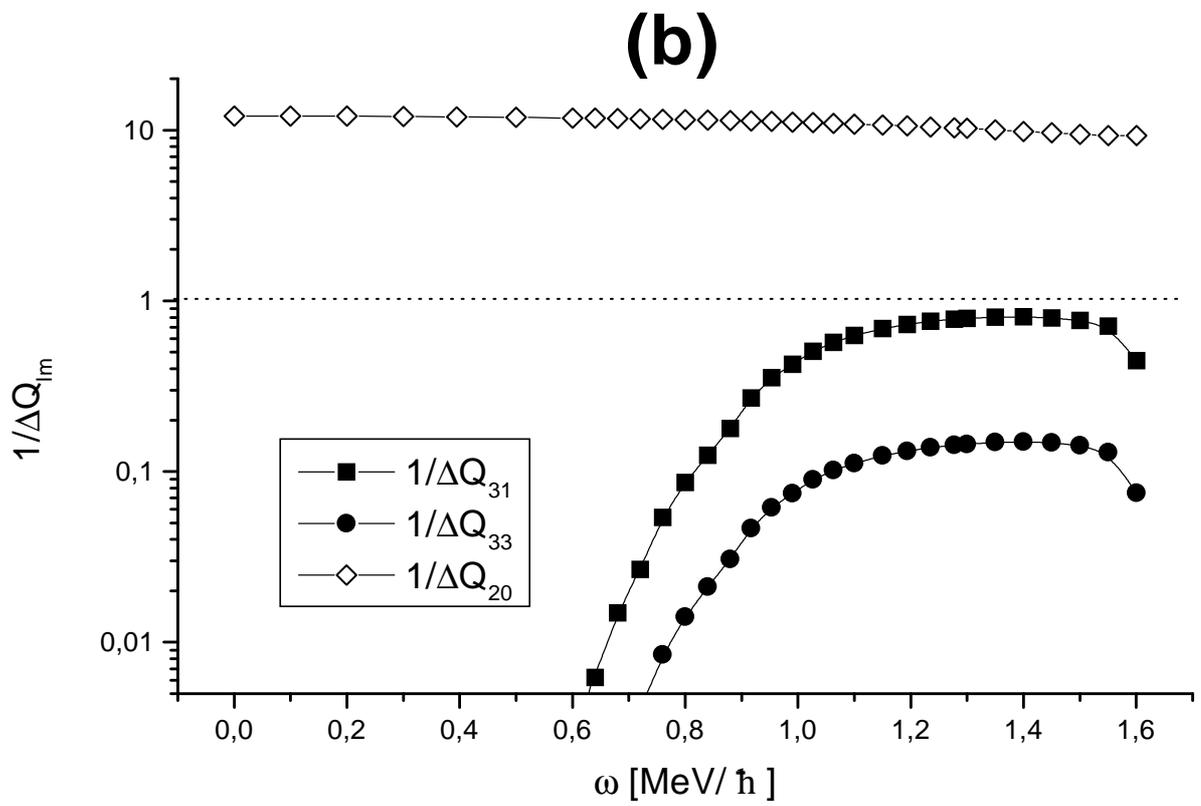
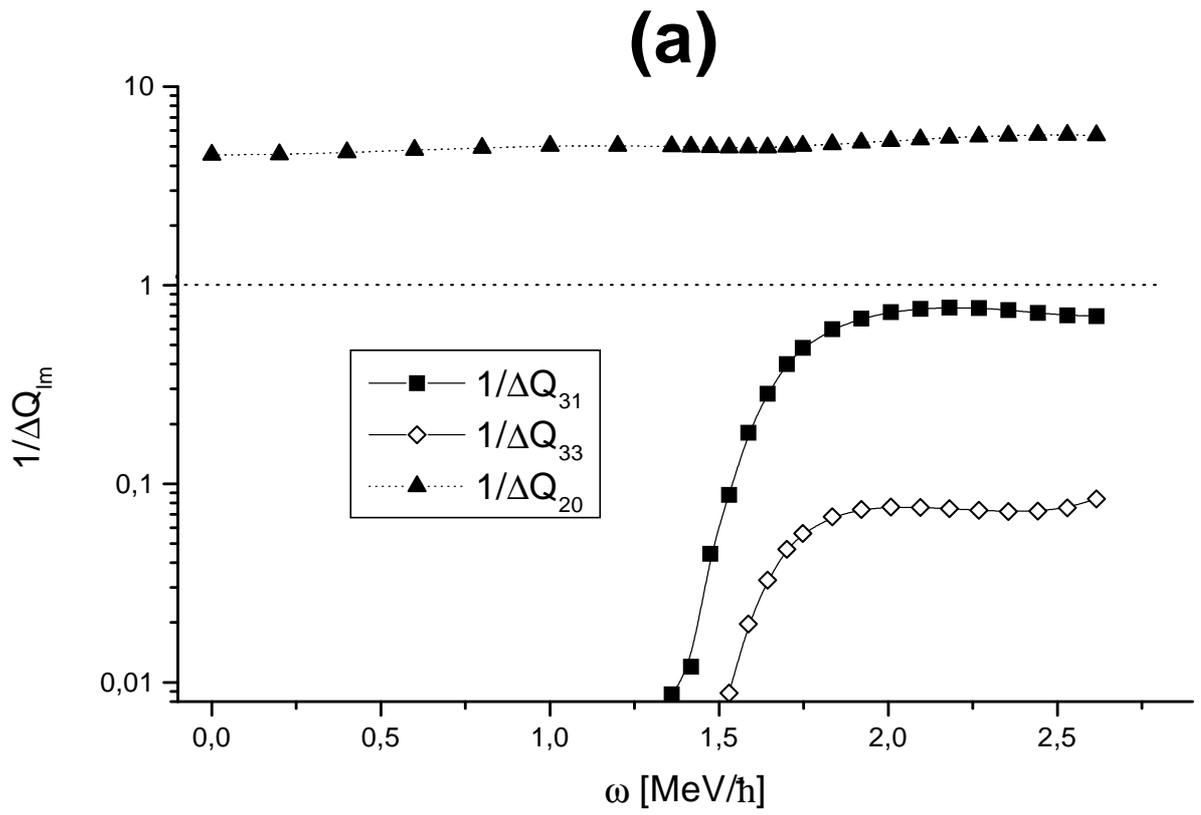


(a)

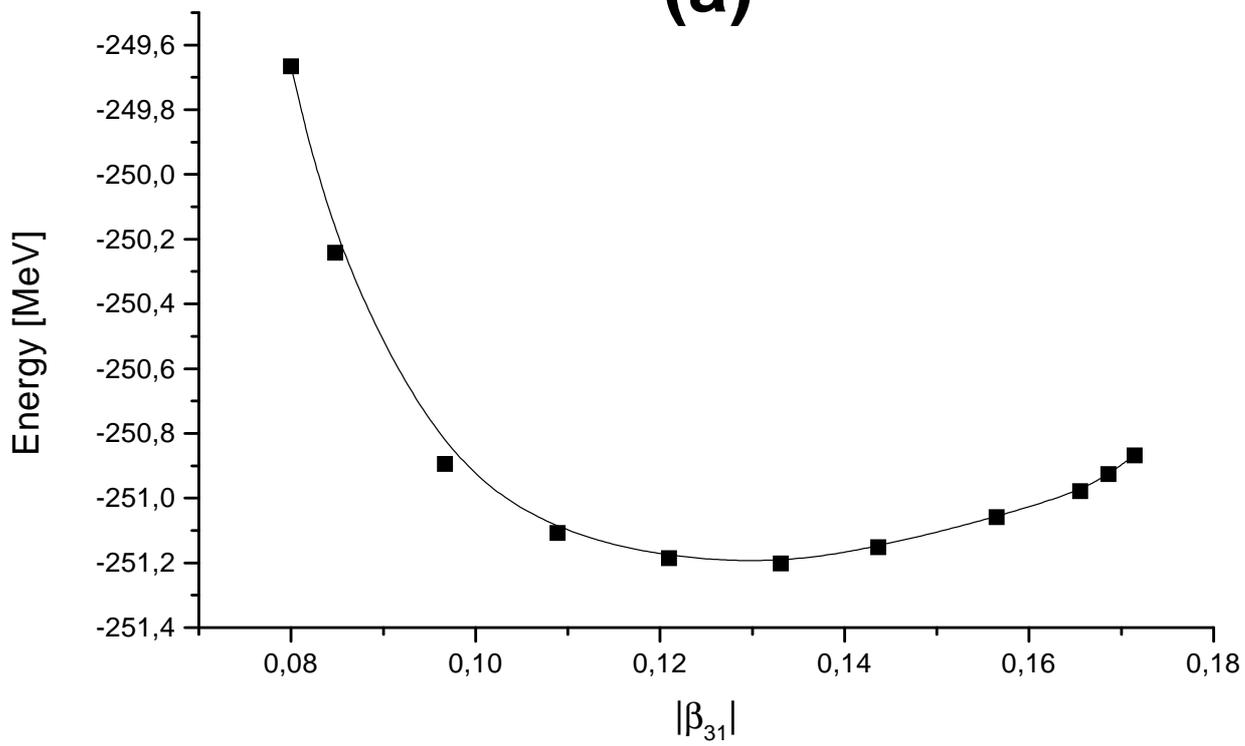


(b)





(a)



(b)

